Soft Matter

PAPER

View Article Online
View Journal | View Issue

Cite this: *Soft Matter*, 2022, **18**, 990

A pressure-jump study on the interaction of osmolytes and crowders with cubic monoolein structures†

Göran Surmeier, Michael Paulus, Eric Schneider, Susanne Dogan,* Metin Tolan and Julia Nase

Many vital processes that take place in biological cells involve remodeling of lipid membranes. These processes take place in a milieu that is packed with various solutes, ranging from ions and small organic osmolytes to proteins and other macromolecules, occupying about 30% of the available volume. In this work, we investigated how molecular crowding, simulated with the polymer polyethylene glycol (PEG), and the osmolytes urea and trimethylamine-*N*-oxide (TMAO) affect the equilibration of cubic monoolein structures after a phase transition from a lamellar state induced by an abrupt pressure reduction. In absence of additives, swollen cubic crystallites form after the transition, releasing excess water over several hours. This process is reflected in a decreasing lattice constant and was monitored with small angle X-ray scattering. We found that the osmotic pressure exerted by PEG and TMAO, which are displaced from narrow inter-bilayer spaces, accelerates the equilibration. When the radius of gyration of the added PEG was smaller than the radius of the water channels of the cubic phase, the effect became more pronounced with increasing molecular weight of the polymers. As the release of hydration water from the cubic structures is accompanied by an increasing membrane curvature and a reduction of the interface between lipids and aqueous phase, urea, which has a slight affinity to reside near membrane surfaces, stabilized the swollen crystallites and slowed down the equilibration dynamics. Our results support the view that cellular solutes are important contributors to dynamic membrane processes, as they can accelerate dehydration of inter-bilayer spaces and promote or counteract membrane curvature.

Received 4th October 2021,
Accepted 4th January 2022

DOI: 10.1039/d1sm01425k

rsc.li/soft-matter-journal

Introduction

Lipid membranes envelope biological cells and divide their interior into compartments and organelles.[1,2] They do not only act as static barriers but undergo remodeling events like fusion and budding to regulate the mass transfer between the separated areas.[3,4] Obviously, membrane composition and various proteins play an important role in such processes.[5,6] It is also known that hydration and curvature of lipid bilayers can strongly be affected by non-specific interactions with solutes in the aqueous environment of membranes.[7–10] The cellular environment contains high amounts of solutes, ranging from ions and organic osmolytes to macromolecules, like proteins, ribosomes, nucleic acids and carbohydrates, occupying about 30% of the available cell volume.[11–13] The presence of a crowded environment shifts chemical equilibria and interaction constants due to the excluded volume effect.[14–17] It was found that crowding can be a driving force of vesicle fusion or budding when background molecules are placed either outside or inside of vesicles.[18–20]

It has long been assumed that organic osmolytes are "background molecules" with the sole purpose to provide the adaptation of a cell to osmotic stress in a hypertonic environment, and have no relevance to cellular processes acting as compatible solutes.[21] In fact, their influence on cellular processes is small compared to other cellular solutes like *e.g.* inorganic ions, which do not interfere with the metabolism only in low concentration ranges.[22] However, it became evident that the compatibility of organic osmolytes is restricted. The influence of different organic osmolytes on the structure and interaction of proteins has been a focal point of research in the last decade.[23–25] While some osmolytes stabilize native states of macromolecules, others act as denaturants. A widely studied couple are trimethylamine-*N*-oxide (TMAO) and urea, which occur in a characteristic ratio of 2 : 1 in many marine species

Fakultät Physik/DELTA, Technische Universität Dortmund, 44221 Dortmund, Germany. E-mail: susanne.dogan@tu-dortmund.de

† Electronic supplementary information (ESI) available. See DOI: 10.1039/d1sm01425k

that are exposed to high osmotic and hydrostatic pressures.[26–30] The interplay of TMAO, which shifts the equilibrium of proteins towards folded states, and urea, which promotes unfolding, is crucial for preserving the functionality of proteins at extreme conditions. TMAO shows strong interactions with water that prevent the molecule from residing in proximity of macromolecules,[31] while interactions of urea with protein backbones and amino acid side chains are favorable.[32,33] Therefore, the presence of these molecules promotes protein structures with either small or large surfaces exposed to the solvent. It was found that the counteracting behavior of TMAO and urea also translates into different interactions with lipid structures and recent studies suggest that the preferential exclusion of molecules like TMAO from interbilayer spaces provides an important contribution to processes of membrane remodeling.[7,8,34–36]

In biological systems, membranes are complex structures built of a variety of different molecules and active fusion processes are driven by proteins. However, this study focusses on basic interactions of lipid layers with solutes and thus a simple model system is applied to identify fundamental effects of additives on hydration and curvature of membranes. Membrane remodeling like fusion and budding involves changes of curvature and the occurrence of non-lamellar lipid structures. Therefore, lipids that form, *e.g.*, bicontinuous cubic or hexagonal phases are a powerful tool to study membrane processes.[37–41] The lipid monoolein forms bicontinuous cubic phases spontaneously in an aqueous medium[42,43] and is a widely studied molecule due to its potential in fields like drug delivery,[44–47] nucleic acid delivery,[48–52] medical imaging,[46,53,54] membrane protein crystallization,[55–59] and biosensing.[60–63] For monoolein/water mixtures, detailed temperature composition phase diagrams exist[43] and also the pressure-dependent behavior was investigated before.[37,64] At ambient pressure and a temperature of 25 °C, monoolein forms the cubic *Pn*3*m* phase in excess water. By the application of hydrostatic pressure, a transition into a lamellar crystalline phase can be triggered.

In this work, we examined the influence of background molecules on membrane processes by studying how crowders and the osmolytes TMAO and urea affect curvature and hydration of cubic monoolein structures. We conducted pressure-jumps across the lamellar to cubic phase boundary at excess water conditions to trigger the formation of a swollen cubic phase. Subsequently, we monitored the diffusion of water from hydration to excess volume by recording the decrease of the cubic lattice constant as a function of time with small angle X-ray scattering (SAXS). Molecular crowding was simulated by adding the polymer polyethylene glycol (PEG) as it was already done in previous studies.[14,23,65,66] We found that the addition of PEG and TMAO reduces the lattice constant of the cubic phase and tends to accelerate the equilibration after a pressure-jump. When the radius of gyration of PEG was smaller than the radius of the water channels of the lipid phase, both effects became more pronounced with increasing molecular weight of the polymers. In contrast, urea slowed the decrease of the lattice constant down, stabilizing lipid structures with large surface areas.

Experimental setup

The pressure-jumps were conducted with a high hydrostatic pressure sample cell designed for X-ray studies.[67] The cell is made of the high tensile strength alloy Inconel 718 and is sealed with diamond windows along the beam path, resisting pressures of up to 5 kbar. The sample liquid is filled into an inner cell that is separated from the pressure transmitting liquid by polyimide windows. The sample temperature was controlled by a circulating water flow and set to 298 K.

Monoolein and buffer solution were poured into the inner sample cell. The substances were mixed mechanically, and the samples were allowed to equilibrate for at least 12 hours. For PEG samples, 10 mM pressure stable BisTris buffer at pH 5 was used and added in concentrations of 80 wt%. PEG of molecular weights between 200 g mol^{-1} and 35 000 g mol^{-1} was dissolved in the buffer solution in concentrations of 150 g L^{-1} before it was mixed with monoolein. For urea and TMAO samples, 10 mM BisTris buffer at pH 7 was used and added in concentrations of 90 wt%. The osmolytes were dissolved in the buffer solution in concentrations of 1 M. For mixtures of urea and TMAO in a 2 : 1 ratio, 0.67 M urea and 0.33 M TMAO were added. All chemicals were purchased from Sigma Aldrich and used as received.

The SAXS experiments were performed at the beamlines BL2[68] and BL9[69] of DELTA (Dortmund, Germany) with photon energies of 12 keV (λ = 1.033 Å) and 13 keV (λ = 0.954 Å) using MAR345 image plate detectors. The beamsize was 0.5 × 0.5 mm^2 at BL2 and 1 × 1 mm^2 at BL9. The setups were calibrated with silver behenate.[70] Pressure-jumps were conducted from between 1 and 2 kbar down to 50 bar. The reduction of pressure took approximately 10 s. After the pressure-jump, SAXS scans were taken at four-minute intervals for several hours. In the cubic phase regime, the exposure time was 150 s and in the lamellar regime, the exposure time was 30 s. The two-dimensional SAXS patterns were integrated azimuthally to obtain the scattering intensity as a function of the wave vector transfer q and an interpolated background was subtracted. Phase behavior and lattice constant a of the sample can then be determined based on Bragg reflections that occur at characteristic ratios of the reciprocal lattice constant $2\pi/a$.[42] The positions of the Bragg reflections were extracted by fitting Gaussian functions.

Results

Fig. 1 shows the pressure-dependent phase behavior of monoolein at excess water conditions upon pressurization and pressure release (left). Moreover, selected integrated SAXS patterns are shown with the obtained fits (right). The Bragg reflections are labelled with the corresponding Miller indices. Exemplary SAXS curves and fits of samples containing additives are presented in the ESI.† In agreement with the results of Czeslik *et al.*,[71] we observed the cubic *Pn*3*m* phase at 50 bar and a transition into a lamellar phase at high pressures. The *inset* provides a more detailed view on the behavior of the cubic

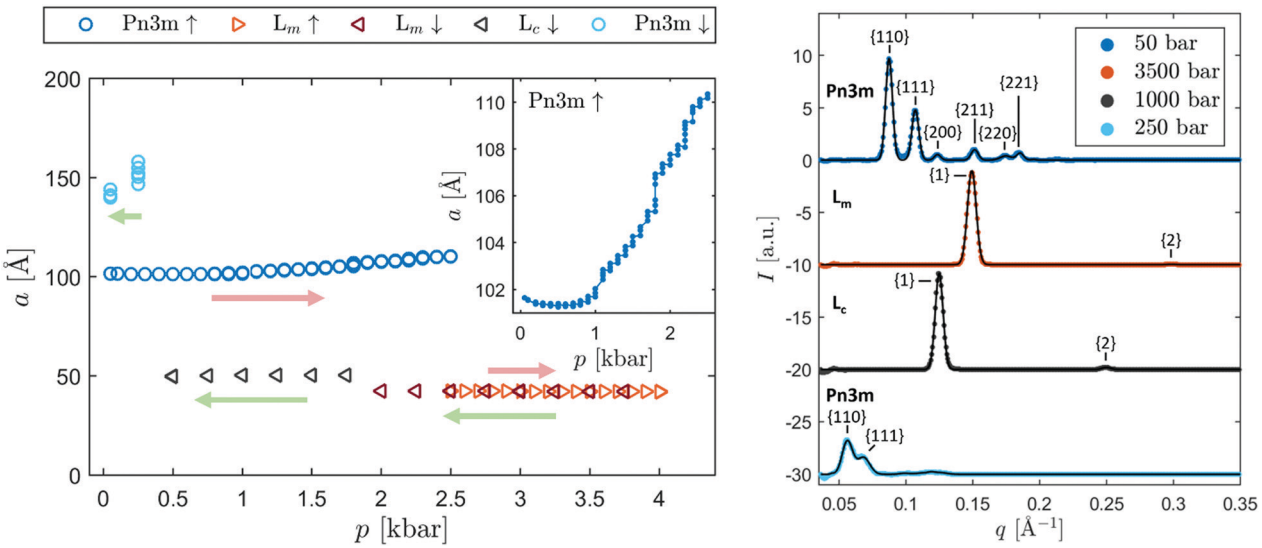

Fig. 1 Left: Phase behavior and lattice parameters *a* of monoolein in excess water upon pressurization (red arrows) and pressure release (green arrows). The *inset* provides a closer look on the lattice constant of the *Pn3m* phase during pressurization, revealing that it increases as a function of time even at constant pressure. The scans were taken at four-minute intervals and the data points are connected to indicate their chronological order. Right: Exemplary integrated SAXS data (colored dots) and fits (black lines) of scans from each phase regime. The Miller indices of the lattice planes that correspond to the observed Bragg reflections are designated.

phase at increasing pressures. Repetitive measurements at four-minute intervals showed that the *Pn3m* phase is not at equilibrium at pressures above 0.5 kbar, as the cubic structures are slowly swelling. Additional measurement series (data not shown) showed that the swelling carries on for many hours or even days at constant pressure until a phase transition into a lamellar phase occurs. Upon pressure release from 4 kbar, a lamellar phase is observed in the corresponding pressure regime, confirming that the cubic phase is not the equilibrium state. However, an instantaneous collapse of the metastable cubic phase could be reliably induced by increasing the pressure above 2.5 kbar.

After the pressure-induced phase transition, a lamellar phase with a spacing of approximately 43 Å formed. During the subsequent release of pressure, a phase transition occurred at 1.75 kbar, as the spacing of the lamellar structures abruptly increased to approximately 49 Å. Since the spacing of both phases barely changed as a function of pressure, it is likely that they exhibit a crystalline chain order. Czeslik *et al.*[71] observed an intermediate phase with a spacing of 43 Å at 7.5 °C upon a pressure-induced cubic *Pn3m* to lamellar transition at 1.4 kbar, before a stable lamellar phase with a spacing of 47 Å formed. They confirmed the crystalline character of the latter phase with wide angle scattering. Qiu and Caffrey[43] found a metastable and a stable lamellar crystalline phase at low temperatures with similar spacings. Consistent with the behavior observed in these studies, we found that the phase with the higher spacing is the equilibrium state in the entire pressure range from 0.5 to 4 kbar, while the phase with the lower spacing is metastable. In the following, we refer to the stable phase as L_c and to the metastable phase as L_m phase. The moment and pressure at which a transition into the stable phase occurred was found to be largely random. However, a reduction of the pressure from more than 2.5 kbar to 1.5 kbar or less reliably induced a transition into the stable L_c phase.

Upon pressure release, the phase transition into the cubic phase occurred between 0.5 and 0.25 kbar. At this point, the cubic phase formed with an increased lattice constant compared to equilibrium. Subsequently, the lattice constant slowly decreased as the cubic structures release excess water.

Based on the described behavior, we applied the following measurement protocol. For each sample, we determined the equilibrium lattice constant of the cubic phase at 50 bar. Then, we increased the pressure to 3.5 kbar to induce a transition into the lamellar phase. After that, we reduced the pressure again, typically to 1 or 1.5 kbar, to trigger the formation of the L_c phase. From this starting point, we performed a pressure-jump back to 50 bar and monitored the decrease of the *Pn3m* lattice constant as a function of time.

The equilibrium lattice constant of monoolein in the *Pn3m* phase at 50 bar upon addition of PEG with different molecular weights is shown in the inset of Fig. 2. The measurement error of the SAXS experiments is below the symbol sizes. The variation of the lattice parameters between the individual samples (circles) is due to the sensitivity of the monoolein samples to external conditions and slow equilibration times. The typical error range for the cubic phase is ±2.5 Å and for the lamellar ±0.3 Å.

If the water content of the lipid phases is known, the length of the lipid molecules in the structure and the size of the water channels can be determined.[42] For monoolein/water mixtures at 25 °C and ambient pressure, the maximum water capacity of the *Pn3m* phase at equilibrium is 44.5 wt%.[43] Based on this value and with the observed mean *Pn3m* lattice constant of

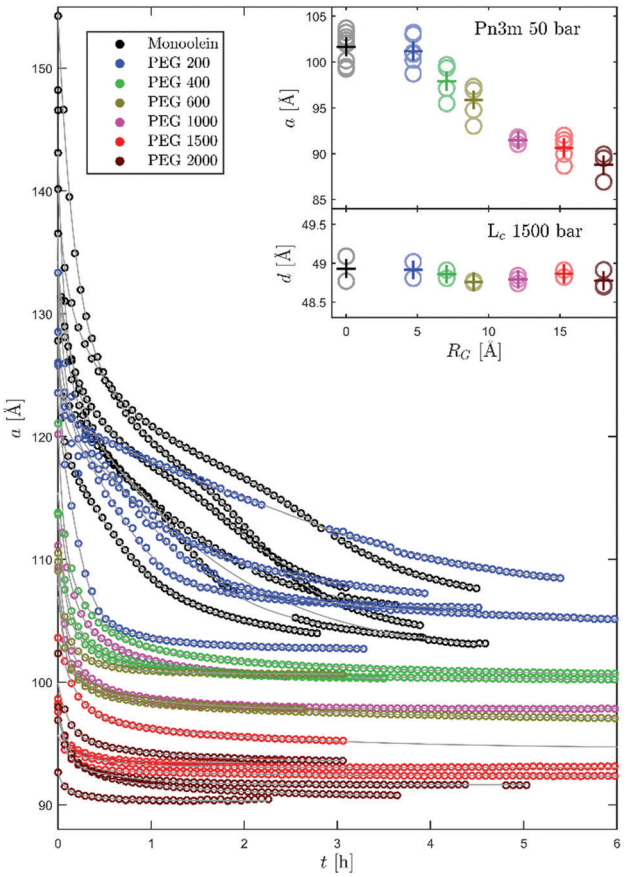

Fig. 2 Decrease of the *Pn3m* lattice constant after a pressure-induced lamellar-to-cubic transition in presence of PEG of different molecular weight as a function of time t (colored symbols) and fits (grey lines). The pressure-jumps were conducted at $t = 0$. The *inset* shows the *Pn3m* lattice constant at 50 bar and the lamellar spacing at 1500 bar before the pressure-jumps as a function of the radius of gyration R_G of the added PEG. The results for pure monoolein are shown at $R_G = 0$ for comparison. The circles represent the obtained values of different samples to illustrate the variance. The crosses mark the mean values.

monoolein in excess water at 50 bar of 102.8 Å, the length of the lipid molecules is determined as approximately 16.1 Å. Assuming that the length of the molecules depends essentially on pressure and temperature, but is barely affected by the addition of PEG, this value can be used to estimate the radii of the water channels r_w of the cubic structures in presence of PEG. Fig. 3 shows the ratio of r_w to the radius of gyration R_G of the added PEG as a function of R_G. With increasing size of the polymers, the cubic structures are more and more compressed. It is known that the osmotic pressure exerted by PEG decreases as a function of its molecular weight at constant mass concentration.[72] However, the osmotic pressure between the water channels of the cubic phase and the excess water regime is determined by the concentration gradient between both regions. Fig. 3 demonstrates that the dimensions of water channels and polymers are in a similar order of magnitude. Therefore, the increasing level of compression with increasing size of the polymers can be explained by an increasing exclusion of PEG from the cubic structures. The larger the PEG molecules are, the more unfavorable the confinement in the cubic structure becomes due to the restriction of the configuration entropy. Once the radius of gyration was larger than the radius of the water channels, we observed the cubic *Ia3d* phase instead of the *Pn3m* phase. In the *Ia3d* regime, no further compression of the lipid phases as a function of R_G occurred, and it can be assumed that the polymers are completely displaced from the water channels.

The *inset* of Fig. 2 shows that the spacing of the lamellar crystalline phase at 1500 bar is largely unaffected by the presence of PEG. Qiu and Caffrey found that the maximum water capacity of the lamellar phase at ambient pressure is approximately 4 wt%.[43] Based on this value, the hydrated interbilayer space can be estimated to be approximately 2 Å thick. Thus, all water molecules that are embedded in the lipid structure are in close proximity to the monoolein headgroups and therefore have limited mobility.[73] Due to the lack of free hydration water, a displacement of water molecules from the lipid structures by osmotic pressure is barely possible. Therefore, the L_c phase is, in contrast to the *Pn3m* phase, not compressed by PEG.

Especially with PEG of higher molecular weights, we observed a formation of cubic structures already at 1000 bar in some cases. Therefore, different starting pressures between 1 and 2 kbar were used for the pressure-jumps. Fig. 2 shows the reduction of the lattice constant of the *Pn3m* phase of monoolein in presence of PEG of different molecular weights after pressure-jumps from the lamellar regime as a function of time. The integrated intensity of the observed Bragg reflections was constant from the second scan on for all samples (see ESI†), indicating that the formation of the *Pn3m* phase was completed in less than four minutes and that the crystallites did not grow considerably during the water release process. Moreover, the width of the reflections at equilibrium was similar for all samples so that it can be assumed that the mean size of the crystallites was largely unaffected by the addition of the polymers.

The equilibration after a pressure-jump accelerated with increasing molecular weight of the added PEG. To compare the speed of the process for different samples, we determined the equilibration times as the time that elapsed after the pressure-jump until the released water volume per second and unit cell fell permanently below a threshold of 30 $Å^3\ s^{-1}$. For this purpose, a smoothed and continuous representation of the data was generated by fitting. We superposed two exponential functions to reproduce the convex decrease of the lattice parameter and a hyperbolic tangent to take into account an intermediate increase of the reduction rate that occurred mainly with pure monoolein. The resulting curves are shown in Fig. 2 as *grey lines*. With the length of the lipid molecules stated above, the water content of the unit cells was determined and by calculating the time derivative, the water release rate was obtained.

Fig. 4 shows the resulting equilibration times as a function of the radius of gyration of the added PEG. The osmotic pressure exerted by the polymers accelerated the equilibration

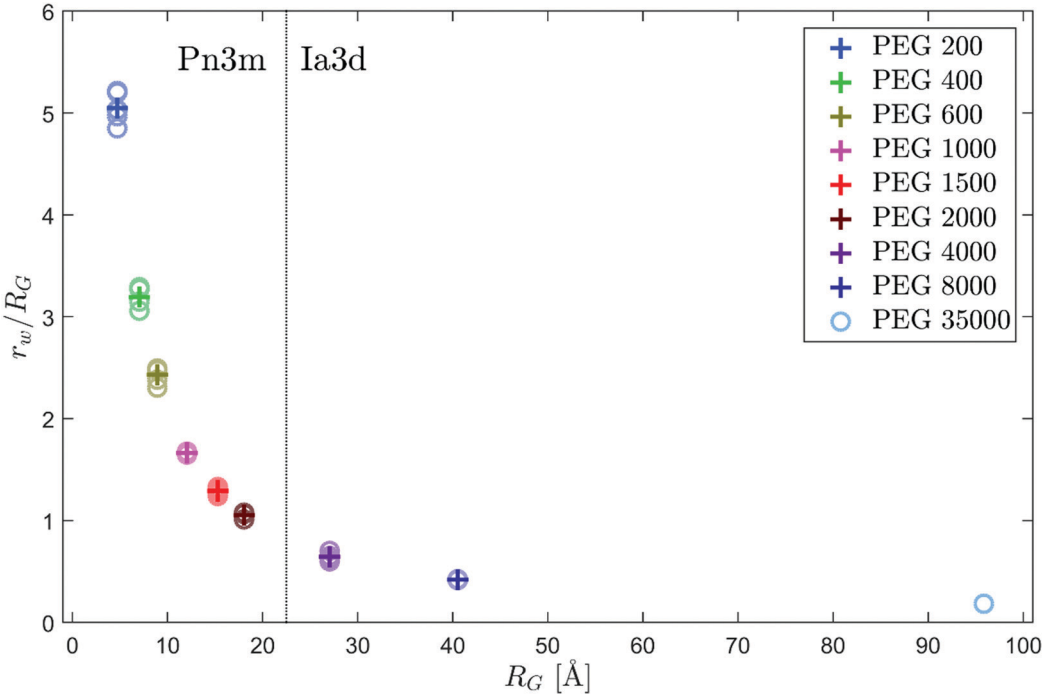

Fig. 3 Ratio of the water channel radius r_w of the *Pn3m* phase at 50 bar to the radius of gyration R_G of the added PEG as a function of R_G. The circles represent the obtained values of different samples to illustrate the variance. The crosses mark the mean values.

process strongly. For pure monoolein, a water release rate of the *Pn3m* unit cells of 30 Å^3 s^{-1} is reached after approximately three hours on average. This value reduces to less than 20 minutes in presence of PEG 2000. While the compression of the lipid structures at equilibrium increases steadily with the size of the polymers, the equilibration time reduces strongly already for PEG 400 and remains on a similar level for larger PEGs showing only a slight downward trend.

In contrast to PEG, urea and TMAO are small molecules with few configurational degrees of freedom. Nevertheless, they also have a strong influence on monoolein structures due to their interactions with water and lipid interfaces. The *inset* of Fig. 5 shows the lattice constant of the *Pn3m* phase at 50 bar and the spacing of the L_c phase at 1000 bar in presence of urea and TMAO before a pressure-jump. In agreement with current knowledge, urea increases the lattice constant as its favorable interactions with the lipid headgroups counteract the negative curvature of the bilayers, whereas TMAO is displaced from the cubic crystallites and compresses the structure due to the resulting osmotic pressure.[7,9,58] The values observed for urea are presumably higher than in equilibrium, as the lattice constant converges to lower values after a pressure-jump. Urea strongly slows down the equilibration dynamics of the cubic phase, so that the waiting time of 12 h between sample preparation and experiment might not be sufficient. From the behavior of the urea samples after a pressure-jump, an equilibrium lattice constant of approximately 110 Å is determined. In a 2 : 1 ratio, the effects of urea and TMAO on the *Pn3m* lattice constant compensate each other and within the range of variance, no difference to pure monoolein is observed. Similar

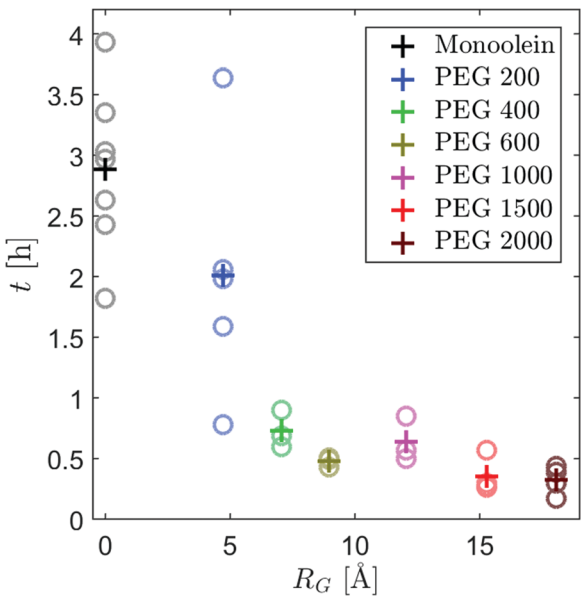

Fig. 4 Period t after a pressure-jump until the released water volume per time and *Pn3m* unit cell decreased below a limit of 30 Å^3 s^{-1} as a function of the radius of gyration R_G of the added PEG as a measure for the speed of the equilibration dynamics. The results for pure monoolein are shown at R_G = 0 for comparison. The *circles* represent the obtained values of different samples to illustrate the variance. The *crosses* mark the mean values.

to PEG, TMAO does not affect the structure of the L_c phase, while urea slightly increases the spacing. An even less pronounced expansion is visible when urea and TMAO are added

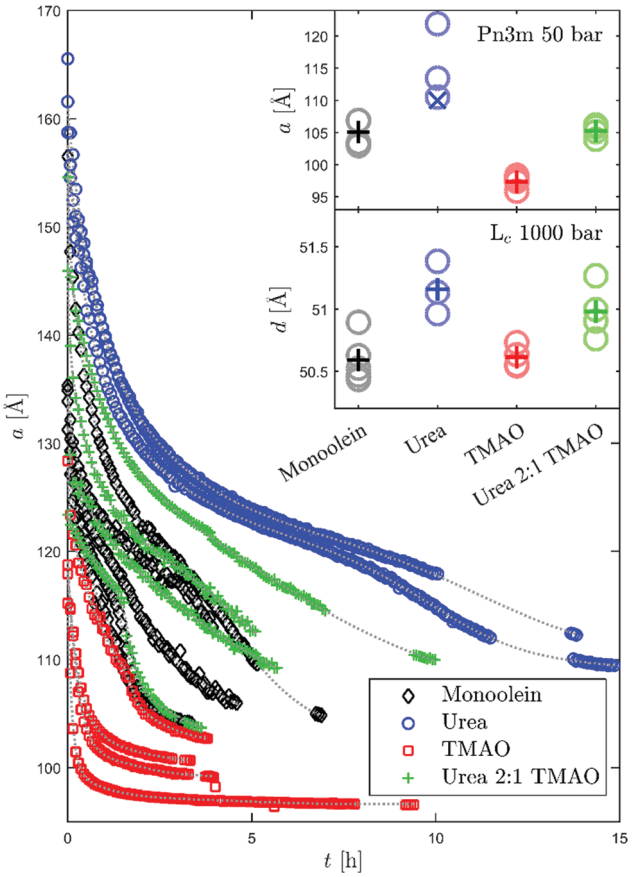

Fig. 5 Decrease of the *Pn3m* lattice constant after a pressure-induced lamellar-to-cubic transition in presence of TMAO and urea as a function of time t (colored symbols) and fits (grey lines). The inset shows the *Pn3m* lattice constant at 50 bar and the lamellar spacing at 1000 bar before the pressure-jumps. The results for pure monoolein are shown at R_G = 0 for comparison. The circles represent the obtained values of different samples to illustrate the variance. The *crosses* mark the mean values. At 50 bar, for urea, the value of the equilibrium lattice constant determined from the convergence after a pressure-jump is indicated with an *'X'* instead.

in a 2 : 1 ratio. In both cases, the expansion is presumably due to urea molecules that enter the narrow interbilayer spaces of the L_c phase, since urea has an affinity to reside at lowly hydrated membrane interfaces.[35,74]

Fig. 5 shows how the addition of urea and TMAO affected the equilibration dynamics of the *Pn3m* phase after a pressure-jump from the lamellar regime. In all cases, the increase of the integrated intensity of the observed Bragg reflections occurred on a much shorter time scale than the reduction of the lattice constant (see ESI†) and the width of the reflections at equilibrium was similar. Thus, it can be assumed that the cubic crystallites formed fast and reached similar dimensions for all samples.

The different interaction mechanisms of the two osmolytes with lipid membranes induced counteracting effects on the water release process. In absence of additives, the equilibration process took five hours on average. Urea strongly reduced the speed of the water-release and after more than 10 hours, the lattice constant was still considerably decreasing. In contrast, for three of four TMAO samples, the reduction of the lattice parameter essentially occurred during the first hour after the pressure-jump. In all cases, TMAO caused an acceleration of the dynamics. The addition of urea and TMAO in a 2 : 1 ratio caused equilibration times that are similar to pure monoolein. However, due to the large fluctuations between the individual samples, it is not possible to conclude whether this ratio provides an optimum compensation of the counteracting effects.

Conclusions

In this work, we investigated the influence of solutes on the equilibration dynamics of cubic monoolein phases. The effect of the size of background molecules on the dehydration of the lipid structures was examined using PEG of different molecular weight. For polymers with a radius of gyration that was smaller than the radius of the *Pn3m* water channels, a linear reduction of the lattice parameter with increasing size was found. Larger PEG induced a phase transition into the *Ia3d* phase. While PEG 200 had only a minor effect on the equilibration dynamics after a pressure-jump, larger polymers strongly accelerated the release of hydration water from swollen cubic crystallites. A faster decrease of the lattice constant was also observed when TMAO was added. In both cases, a preferred displacement of the solutes from the lipid structures induces an osmotic pressure between hydration and excess water regime. Residing in the confined hydration volume of the cubic crystallites is unfavorable for PEG due to the restriction of the configuration entropy that increases with the size of the polymers. In contrast, TMAO is a small and rigid molecule that is displaced from membrane interfaces due to its dipole moment and strong interactions with water.[7] The dehydration of inter-bilayer spaces is a prerequisite for membrane fusion. Therefore, the observed ability of PEG and TMAO to accelerate the dehydration of lipid structure indicates that the presence of both substances promotes fusion.

Urea has an affinity to interact with bilayer surfaces.[32,33] In this work, we demonstrated that it stabilizes swollen *Pn3m* structures and reduces the speed of the equilibration dynamics after pressure-jumps across the lamellar-to-cubic phase boundary. Intermediate states of membrane fusion are characterized by high negative curvature. Our experiments show that urea counteracts the formation of such structures. In a 2 : 1 ratio, the effects of urea and TMAO compensated each other to a large extend.

Our results support the view that cellular solutes contribute to membrane processes that involve changes of the curvature of lipid layers or require dehydration of inter-bilayer spaces.[7,8] This work shows that background molecules can either increase or reduce barriers for membrane remodeling.

Author contributions

G. S., J. N. and M. P. designed research. G. S., E. S., S. D. and M. P. performed research. G. S. analyzed data. G. S. and S. D. wrote the paper with contributions from the co-authors.

Conflicts of interest

There are no conflicts to declare.

Acknowledgements

The authors thank the DELTA machine group for providing synchrotron radiation and the Deutsche Forschungsgemeinschaft (FOR 1979) for financial support. This work was supported by RESOLV, funded by the Deutsche Forschungsgemeinschaft (DFG, German Research Foundation) under Germany's Excellence Strategy – EXC 2033 – 390677874 – RESOLV.

References

1 D. Casares, P. V. Escribá and C. A. Rosselló, Membrane lipid composition: effect on membrane and organelle structure, function and compartmentalization and therapeutic avenues, *Int. J. Mol. Sci.*, 2019, **20**, 2167.
2 S. Cohen, A. M. Valm and J. Lippincott-Schwartz, Interacting organelles, *Curr. Opin. Cell Biol.*, 2018, **53**, 84–91.
3 T. Farmer, N. Naslavsky and S. Caplan, Tying trafficking to fusion and fission at the mighty mitochondria, *Traffic*, 2018, **19**, 569–577.
4 V. Haucke and M. M. Kozlov, Membrane remodeling in clathrin-mediated endocytosis, *J. Cell Sci.*, 2018, **131**, jcs216812.
5 S. Halldorsson, S. Li, M. Li, K. Harlos, T. A. Bowden and J. T. Huiskonen, Shielding and activation of a viral membrane fusion protein, *Nat. Commun.*, 2018, **9**, 1–9.
6 R. B. Lira, T. Robinson, R. Dimova and K. A. Riske, Highly efficient protein-free membrane fusion: a giant vesicle study, *Biophys. J.*, 2019, **116**, 79–91.
7 S. Sukenik, S. Dunsky, A. Barnoy, I. Shumilin and D. Harries, TMAO mediates effective attraction between lipid membranes by partitioning unevenly between bulk and lipid domains, *Phys. Chem. Chem. Phys.*, 2017, **19**, 29862–29871.
8 M. Manisegaran, S. Bornemann, I. Kiesel and R. Winter, Effects of the deep-sea osmolyte TMAO on the temperature and pressure dependent structure and phase behavior of lipid membranes, *Phys. Chem. Chem. Phys.*, 2019, **21**, 18533–18540.
9 H. Takahashi, A. Matsuo and I. Hatta, Effects of chaotropic and kosmotropic solutes on the structure of lipid cubic phase: Monoolein-water systems, *Mol. Cryst. Liq. Cryst. Sci. Technol., Sect. A*, 2000, **347**, 231–238.
10 S. R. Al-Ayoubi, P. K. Schinkel, M. Berghaus, M. Herzog and R. Winter, Combined effects of osmotic and hydrostatic pressure on multilamellar lipid membranes in the presence of PEG and trehalose, *Soft Matter*, 2018, **14**, 8792–8802.
11 S. B. Zimmerman and S. O. Trach, Estimation of macromolecule concentrations and excluded volume effects for the cytoplasm of Escherichia coli, *J. Mol. Biol.*, 1991, **222**, 599–620.
12 R. J. Ellis and A. P. Minton, Join the crowd, *Nature*, 2003, **425**, 27–28.
13 A. B. Fulton, How crowded is the cytoplasm?, *Cell*, 1982, **30**, 345–347.
14 K. Julius, J. Weine, M. Gao, J. Latarius, M. Elbers, M. Paulus, M. Tolan and R. Winter, Impact of Macromolecular Crowding and Compression on Protein–Protein Interactions and Liquid–Liquid Phase Separation Phenomena, *Macromolecules*, 2019, **52**, 1772–1784.
15 H.-X. Zhou, G. Rivas and A. P. Minton, Macromolecular crowding and confinement: biochemical, biophysical, and potential physiological consequences, *Annu. Rev. Biophys.*, 2008, **37**, 375–397.
16 A. P. Minton, The influence of macromolecular crowding and macromolecular confinement on biochemical reactions in physiological media, *J. Biol. Chem.*, 2001, **276**, 10577–10580.
17 P. H. Schummel, M. Gao and R. Winter, Modulation of the Polymerization Kinetics of α/β-Tubulin by Osmolytes and Macromolecular Crowding, *ChemPhysChem*, 2017, **18**, 189–197.
18 H. Terasawa, K. Nishimura, H. Suzuki, T. Matsuura and T. Yomo, Coupling of the fusion and budding of giant phospholipid vesicles containing macromolecules, *Proc. Natl. Acad. Sci. U. S. A.*, 2012, **109**, 5942–5947.
19 B. R. Lentz, PEG as a tool to gain insight into membrane fusion, *Eur. Biophys. J.*, 2007, **36**, 315–326.
20 S. Hui, T. Kuhl, Y. Guo and J. Israelachvili, Use of poly (ethylene glycol) to control cell aggregation and fusion, *Colloids Surf., B*, 1999, **14**, 213–222.
21 P. H. Yancey, Organic osmolytes as compatible, metabolic and counteracting cytoprotectants in high osmolarity and other stresses, *J. Exp. Biol.*, 2005, **208**, 2819–2830.
22 P. H. Yancey, Water stress, osmolytes and proteins, *Am. Zool.*, 2001, **41**, 699–709.
23 K. Julius, S. R. Al-Ayoubi, M. Paulus, M. Tolan and R. Winter, The effects of osmolytes and crowding on the pressure-induced dissociation and inactivation of dimeric LADH, *Phys. Chem. Chem. Phys.*, 2018, **20**, 7093–7104.
24 N. Smolin, V. P. Voloshin, A. V. Anikeenko, A. Geiger, R. Winter and N. N. Medvedev, TMAO and urea in the hydration shell of the protein SNase, *Phys. Chem. Chem. Phys.*, 2017, **19**, 6345–6357.
25 A. Rani and P. Venkatesu, Changing relations between proteins and osmolytes: a choice of nature, *Phys. Chem. Chem. Phys.*, 2018, **20**, 20315–20333.
26 V. Voloshin, N. Smolin, A. Geiger, R. Winter and N. N. Medvedev, Dynamics of TMAO and urea in the hydration shell of the protein SNase, *Phys. Chem. Chem. Phys.*, 2019, **21**, 19469–19479.
27 P. Ganguly, J. Polák, N. F. A. van der Vegt, J. Heyda and J.-E. Shea, Protein Stability in TMAO and Mixed Urea–TMAO Solutions, *J. Phys. Chem. B*, 2020, **124**, 6181–6197.
28 D. R. Canchi and A. E. García, Cosolvent effects on protein stability, *Annu. Rev. Phys. Chem.*, 2013, **64**, 273–293.

29 J. R. Treberg, B. Speers-Roesch, P. M. Piermarini, Y. K. Ip, J. S. Ballantyne and W. R. Driedzic, The accumulation of methylamine counteracting solutes in elasmobranchs with differing levels of urea: a comparison of marine and freshwater species, *J. Exp. Biol.*, 2006, **209**, 860–870.
30 T.-Y. Lin and S. N. Timasheff, Why do some organisms use a urea-methylamine mixture as osmolyte? Thermodynamic compensation of urea and trimethylamine N-oxide interactions with protein, *Biochemistry*, 1994, **33**, 12695–12701.
31 D. Bolen and I. V. Baskakov, The osmophobic effect: natural selection of a thermodynamic force in protein folding, *J. Mol. Biol.*, 2001, **310**, 955–963.
32 M. C. Stumpe and H. Grubmüller, Interaction of urea with amino acids: implications for urea-induced protein denaturation, *J. Am. Chem. Soc.*, 2007, **129**, 16126–16131.
33 D. R. Canchi and A. E. García, Backbone and side-chain contributions in protein denaturation by urea, *Biophys. J.*, 2011, **100**, 1526–1533.
34 J. Valerio, S. Bernstorff and S. Funari, Effect of urea and tmao on lipid bilayers, *Eur. Pharm. J.*, 2017, **64**, 24–27.
35 Q. D. Pham, A. Wolde-Kidan, A. Gupta, A. Schlaich, E. Schneck, R. R. Netz and E. Sparr, Effects of Urea and TMAO on Lipid Self-Assembly under Osmotic Stress Conditions, *J. Phys. Chem. B*, 2018, **122**, 6471–6482.
36 J. A. Mondal, Effect of trimethylamine N-oxide on interfacial electrostatics at phospholipid monolayer–water interfaces and its relevance to cardiovascular disease, *J. Phys. Chem. Lett.*, 2016, **7**, 1704–1708.
37 A. Levin, C. Jeworrek, R. Winter, K. Weise and C. Czeslik, Lipid Phase Control and Secondary Structure of Viral Fusion Peptides Anchored in Monoolein Membranes, *J. Phys. Chem. B*, 2017, **121**, 8492–8502.
38 D. P. Siegel, Fourth-Order Curvature Energy Model for the Stability of Bicontinuous Inverted Cubic Phases in Amphiphile- Water Systems, *Langmuir*, 2010, **26**, 8673–8683.
39 M. Chavarha, H. Khoojinian, L. E. Schulwitz Jr, S. C. Biswas, S. B. Rananavare and S. B. Hall, Hydrophobic surfactant proteins induce a phosphatidylethanolamine to form cubic phases, *Biophys. J.*, 2010, **98**, 1549–1557.
40 B. G. Tenchov, R. C. MacDonald and B. R. Lentz, Fusion peptides promote formation of bilayer cubic phases in lipid dispersions. An x-ray diffraction study, *Biophys. J.*, 2013, **104**, 1029–1037.
41 T.-Y. D. Tang, N. J. Brooks, C. Jeworrek, O. Ces, N. J. Terrill, R. Winter, R. H. Templer and J. M. Seddon, Hydrostatic Pressure Effects on the Lamellar to Gyroid Cubic Phase Transition of Monolinolein at Limited Hydration, *Langmuir*, 2012, **28**, 13018–13024.
42 C. V. Kulkarni, W. Wachter, G. Iglesias-Salto, S. Engelskirchen and S. Ahualli, Monoolein: a magic lipid?, *Phys. Chem. Chem. Phys.*, 2011, **13**, 3004–3021.
43 H. Qiu and M. Caffrey, The phase diagram of the monoolein/water system: metastability and equilibrium aspects, *Biomaterials*, 2000, **21**, 223–234.
44 A. Ganem-Quintanar, D. Quintanar-Guerrero and P. Buri, Monoolein: a review of the pharmaceutical applications, *Drug Dev. Ind. Pharm.*, 2000, **26**, 809–820.
45 J. C. Shah, Y. Sadhale and D. M. Chilukuri, Cubic phase gels as drug delivery systems, *Adv. Drug Delivery Rev.*, 2001, **47**, 229–250.
46 X. Mulet, B. J. Boyd and C. J. Drummond, Advances in drug delivery and medical imaging using colloidal lyotropic liquid crystalline dispersions, *J. Colloid Interface Sci.*, 2013, **393**, 1–20.
47 E. Nazaruk, P. Miszta, S. Filipek, E. Górecka, E. M. Landau and R. Bilewicz, Lyotropic cubic phases for drug delivery: diffusion and sustained release from the mesophase evaluated by electrochemical methods, *Langmuir*, 2015, **31**, 12753–12761.
48 I. Lopes, A. C. N. Oliveira, M. P. Sária, J. P. Neves Silva, O. Gonçalves, A. C. Gomes and M. E. C. Real Oliveira, Monoolein-based nanocarriers for enhanced folate receptor-mediated RNA delivery to cancer cells, *J. Liposome Res.*, 2016, **26**, 199–210.
49 C. Leal, N. F. Bouxsein, K. K. Ewert and C. R. Safinya, Highly efficient gene silencing activity of siRNA embedded in a nanostructured gyroid cubic lipid matrix, *J. Am. Chem. Soc.*, 2010, **132**, 16841–16847.
50 H. Kim and C. Leal, Cuboplexes: Topologically active siRNA delivery, *ACS Nano*, 2015, **9**, 10214–10226.
51 M. Kang and C. Leal, Soft Nanostructured Films for Actuated Surface-Based siRNA Delivery, *Adv. Funct. Mater.*, 2016, **26**, 5610–5620.
52 H. Kim, J. Sung, Y. Chang, A. Alfeche and C. Leal, Microfluidics synthesis of gene silencing cubosomes, *ACS Nano*, 2018, **12**, 9196–9205.
53 A. Gupta, T. Stait-Gardner, L. De Campo, L. J. Waddington, N. Kirby, W. S. Price and M. J. Moghaddam, Nanoassemblies of Gd–DTPA–monooleyl and glycerol monooleate amphiphiles as potential MRI contrast agents, *J. Mater. Chem. B*, 2014, **2**, 1225–1233.
54 U. Bazylińska, J. Kulbacka, J. Schmidt, Y. Talmon and S. Murgia, Polymer-free cubosomes for simultaneous bioimaging and photodynamic action of photosensitizers in melanoma skin cancer cells, *J. Colloid Interface Sci.*, 2018, **522**, 163–173.
55 A. Zabara, J. T. Y. Chong, I. Martiel, L. Stark, B. A. Cromer, C. Speziale, C. J. Drummond and R. Mezzenga, Design of ultra-swollen lipidic mesophases for the crystallization of membrane proteins with large extracellular domains, *Nat. Commun.*, 2018, **9**, 1–9.
56 C.-Y. Huang, V. Olieric, P. Ma, E. Panepucci, K. Diederichs, M. Wang and M. Caffrey, In meso in situ serial X-ray crystallography of soluble and membrane proteins, *Acta Crystallogr., Sect. D: Biol. Crystallogr.*, 2015, **71**, 1238–1256.
57 V. Cherezov, Lipidic cubic phase technologies for membrane protein structural studies, *Curr. Opin. Struct. Biol.*, 2011, **21**, 559–566.

58 V. Cherezov, J. Clogston, M. Z. Papiz and M. Caffrey, Room to move: crystallizing membrane proteins in swollen lipidic mesophases, *J. Mol. Biol.*, 2006, **357**, 1605–1618.
59 V. Cherezov, J. Clogston, Y. Misquitta, W. Abdel-Gawad and M. Caffrey, Membrane protein crystallization in meso: lipid type-tailoring of the cubic phase, *Biophys. J.*, 2002, **83**, 3393–3407.
60 V. Grippo, S. Ma, R. Ludwig, L. Gorton and R. Bilewicz, Cellobiose dehydrogenase hosted in lipidic cubic phase to improve catalytic activity and stability, *Bioelectrochemistry*, 2019, **125**, 134–141.
61 W. Sun, J. J. Vallooran, W.-K. Fong and R. Mezzenga, Lyotropic liquid crystalline cubic phases as versatile host matrices for membrane-bound enzymes, *J. Phys. Chem. Lett.*, 2016, **7**, 1507–1512.
62 J. J. Vallooran, S. Handschin, S. M. Pillai, B. N. Vetter, S. Rusch, H.-P. Beck and R. Mezzenga, Lipidic cubic phases as a versatile platform for the rapid detection of biomarkers, viruses, bacteria, and parasites, *Adv. Funct. Mater.*, 2016, **26**, 181–190.
63 E. Nazaruk, R. Bilewicz, G. Lindblom and B. Lindholm-Sethson, Cubic phases in biosensing systems, *Anal. Bioanal. Chem.*, 2008, **391**, 1569.
64 R. Winter, Effects of hydrostatic pressure on lipid and surfactant phases, *Curr. Opin. Colloid Interface Sci.*, 2001, **6**, 303–312.
65 N. F. Dupuis, E. D. Holmstrom and D. J. Nesbitt, Molecular-crowding effects on single-molecule RNA folding/unfolding thermodynamics and kinetics, *Proc. Natl. Acad. Sci. U. S. A.*, 2014, **111**, 8464–8469.
66 J. Tyrrell, K. M. Weeks and G. J. Pielak, Challenge of mimicking the influences of the cellular environment on RNA structure by PEG-induced macromolecular crowding, *Biochemistry*, 2015, **54**, 6447–6453.
67 F. J. Wirkert, M. Paulus, J. Nase, J. Möller, S. Kujawski, C. Sternemann and M. Tolan, X-ray reflectivity measurements of liquid/solid interfaces under high hydrostatic pressure conditions, *J. Synchrotron Radiat.*, 2014, **21**, 76–81.
68 E. Schneider, M. Paulus, T. Witt, J. Bolle, H. Leif, M. Kowalski, W. Tillmann and M. Tolan, The new wide and small angle scattering setup at beamline BL2 of DELTA, *DELTA Annu. Rep.*, 2019, **2019**, 21–22.
69 C. Krywka, C. Sternemann, M. Paulus, N. Javid, R. Winter, A. Al-Sawalmih, S. Yi, D. Raabe and M. Tolan, The small-angle and wide-angle X-ray scattering set-up at beamline BL9 of DELTA, *J. Synchrotron Radiat.*, 2007, **14**, 244–251.
70 T. Huang, H. Toraya, T. Blanton and Y. Wu, X-ray powder diffraction analysis of silver behenate, a possible low-angle diffraction standard, *J. Appl. Crystallogr.*, 1993, **26**, 180–184.
71 C. Czeslik, R. Winter, G. Rapp and K. Bartels, Temperature- and pressure-dependent phase behavior of monoacylglycerides monoolein and monoelaidin, *Biophys. J.*, 1995, **68**, 1423–1429.
72 N. P. Money, Osmotic pressure of aqueous polyethylene glycols: relationship between molecular weight and vapor pressure deficit, *Plant Physiol.*, 1989, **91**, 766–769.
73 T. Yamada, N. Takahashi, T. Tominaga, S. Takata and H. Seto, Dynamical behavior of hydration water molecules between phospholipid membranes, *J. Phys. Chem. B*, 2017, **121**, 8322–8329.
74 A. Nowacka, S. Douezan, L. Wadsö, D. Topgaard and E. Sparr, Small polar molecules like glycerol and urea can preserve the fluidity of lipid bilayers under dry conditions, *Soft Matter*, 2012, **8**, 1482–1491.